



Contents lists available at ScienceDirect

Arabian Journal of Chemistry

journal homepage: www.ksu.edu.saCd-CeO₂@C: Synthesis via consumption of Cd²⁺ and organic pollutants and removal of organic pollutantsHeyun Tan^{a,1}, Yuantao Cai^{a,1}, Gangfeng Liang^a, Paolo Aprea^b, Shiyu Hao^{a,*}^a Xingzhi College, College of Chemistry and Materials Science, Zhejiang Normal University, Jinhua 321004, China^b Department of Chemical, Materials and Production Engineering, University Federico II, P.le V. Tecchio 80, 80125 Naples, Italy

ARTICLE INFO

Keywords:
Organic dyes
Heavy metal ions
Cd-CeO₂@C
Carbon bond
Photocatalysis

ABSTRACT

In this study, a Cd-CeO₂@C photocatalyst was produced via the calcination of a precursor (Cd-Ce(OH)₄@AR14) obtained by co-precipitation of Ce(NO₃)₃·6H₂O, Cd(NO₃)₂·4H₂O and acid red 14 (AR14). The structure, composition, morphology, and optical properties of the synthesized products were characterized by X-ray diffraction (XRD), scanning electron microscopy (SEM), infrared spectrum (FT-IR), Ultraviolet-Visible Diffuse Reflectance Spectroscopy (UV-Vis DRS), X-ray photoelectron spectroscopy (XPS) and Photoluminescence Spectroscopy (PL). The photocatalytic activity of the synthesized materials was evaluated by performing the degradation of AR14. The results showed that the band gap of CeO₂ could be effectively reduced by Cd-doping, and that carbon bonds could decrease the recombination rate of photogenerated electrons and holes, resulting in enhancing the photocatalytic efficiency of the synthesized materials compared with that of pure CeO₂. Hydroxyl groups play an important role in the photocatalysis because the adsorption of AR14 over Cd-CeO₂@C is greatly affected by the content of hydroxyl groups. Moreover, effect of oxygen vacancies on the photocatalytic efficiency was investigated and the results showed that oxygen vacancies could improve the photocatalytic efficiency of the resulted samples.

1. Introduction

Nowadays, synthetic dyes are widely used in textile, leather, coating, dyeing and other industries. As a result, a large volume of dye-containing wastewater not thoroughly treated are emitted to the environment, causing serious harm (Bilińska et al., 2016). At present, adsorption (Bello et al., 2015), membrane filtration (Rashidi et al., 2015), biodegradation (Elumalai et al., 2021), chemical oxidation (Yao et al., 2016), etc. have been used to remove dyes wastewater. However, these methods have some disadvantages, such as high cost, complex plant design and operation, long processing cycle, probable secondary pollution, etc. It is reported that photocatalysis technology could degrade organic pollutants through the activity of radical species such as hydroxyl radical, superoxide radical, and photogenerated holes. Recently, many researchers have focused their attention on photocatalysis and piezo-photocatalysis due to its low cost, environmental compatibility, and efficient removal of pollutants (Bueno-Alejo et al., 2021, zhang et al., 2022, wang et al., 2023). At present, the most used

photocatalysts are TiO₂, ZnO, CeO₂, WO₃ etc. (Zhuang et al., 2017, Kumar et al., 2021, Fang et al., 2015, Tahir et al., 2019).

Among them, CeO₂ has attracted much attention due to its unique 4f electronic structure, high chemical stability, strong redox ability, and easy occurrence of oxygen vacancies (Fang et al., 2015, Subramanyam et al., 2020). However, the application of pure CeO₂ is limited due to its wide band gap (about 3.2 eV), low utilization of visible light and low carrier mobility (Zeng et al., 2015). The photocatalytic efficiency of CeO₂ can be improved by modifying its structure with several techniques, such as doping with metal or non-metal ions, precious metal deposition, formation of complexes etc. (Ma et al., 2019). Some studies have shown that doping CeO₂ with ions can accelerate the charge separation and expand the light absorption spectral range, which is an effective way to improve the photocatalytic efficiency of semiconductors (Miao et al., 2016). Gnanam et al. found that Cd²⁺ doping can effectively improve the degradation rate of organic dyes (Gnanam and Rajendran, 2018). Later, Murugadoss et al. investigated the effect of doping with different metal ions on the photocatalytic efficiency of CeO₂ and

Peer review under responsibility of King Saud University.

* Corresponding author.

E-mail address: sky54@zjnu.cn (S. Hao).¹ Heyun Tan and yuantao Cai, equally contributed to this paper, are the co-first authors.<https://doi.org/10.1016/j.arabjc.2023.105496>

Received 16 September 2023; Accepted 26 November 2023

Available online 28 November 2023

1878-5352/© 2023 The Authors. Published by Elsevier B.V. on behalf of King Saud University. This is an open access article under the CC BY-NC-ND license (<http://creativecommons.org/licenses/by-nc-nd/4.0/>).

furtherly proved the effect of Cd^{2+} (Murugadoss et al., 2019). Although Cd^{2+} -doping can change the band gap of ceria and improve the utilization of the adsorbed light energy, such a photocatalyst is still not ideal for adsorbing pollutants and improving the separation efficiency of photogenerated electrons and holes. It was reported that combining the ceria with carbon-based materials could effectively accelerate the electron-hole separation rate because of the carbon bonds formed in the catalyst (Qian et al., 2018). Xu et al. combined CeO_2 with graphite carbon nitride ($\text{g-C}_3\text{N}_4$) by means of a one-pot hydrothermal synthesis process and found that: (i) C-doping could effectively improve the utilization of sunlight and the reduction ability of photogenerated electrons; (ii) low loading of carbon could effectively promote the migration of photogenerated electrons and improve the specific surface area of materials (Xu et al., 2021). Another ceria/carbon-based photocatalyst, CeO_2/rGO (rGO: reduced graphene oxide) was synthesized by Murali et al., who reported that its photocatalytic efficiency was significantly improved because rGO acts as an electron acceptor and effectively promotes the separation and transmission of electron-hole pairs (Murali et al., 2019).

It was also reported that the photocatalytic efficiency could be further improved by introducing C and Cd into the photocatalysts at the same time. Azqhandi et al. synthesized Cd^{2+} doped ZnO/CNT (CNT: carbon nanotubes) composites by a microwave-assisted hydrothermal method. The resulted composite showed a high photocatalytic degradation efficiency of methylene orange due to its efficient adsorption behavior, unique mesoporous surface of CNT and lower band gap (Azqhandi et al., 2017). Karimi et al. prepared a new photocatalyst ($\text{NiO}/\text{Cd}/\text{g-C}_3\text{N}_4$) by microwave-assisted method. The material showed excellent activity for the degradation of methylene blue, mainly attributed to its low band gap, improved photogenerated electron-hole separation efficiency, and good visible light absorption (Karimi et al., 2020). Based on the above data, it can be inferred that the photocatalysis efficiency of CeO_2 can be further improved by introducing C and Cd at the same time. However, the scalability of the catalyst production can be hampered by the fact that the most used carbon sources are commercial ones (such as carbon nanotubes, graphene, $\text{g-C}_3\text{N}_4$, etc.), that results in high costs and weak carbon-ceria adhesion (Wang et al., 2020). In addition, Cd is usually introduced in the form of chemicals, which can further increase the synthesis cost and easily cause heavy metals pollution. In this frame, the possibility of using raw materials recovered from waste, with the aim of both finding a simple way to efficiently introduce C and Cd into CeO_2 and keeping the synthesis cost low, appears very appealing. Interestingly, some research report that wastewater containing dyes can often contain heavy metal ions such as Cd^{2+} , Ni^{2+} , Cu^{2+} (Velusamy et al., 2021). Using such wastewater for the preparation of photocatalysts would hit the double target of lowering the synthesis cost while recycling a waste. Based on this assumption, a $\text{Cd-CeO}_2/\text{C}$ photocatalyst was synthesized starting from acid red 14 (AR14, used as C source) and cadmium nitrate tetrachloride (used as Cd source), selected as simulant of typical pollutants present in dye industry wastewaters. The catalyst was produced (Fig. S1) via calcination under N_2 atmosphere of a precursor ($\text{Cd-Ce}(\text{OH})_4/\text{AR14}$) obtained by inducing a coprecipitation in a Ce^{3+} , Cd^{2+} and AR14 solution. The obtained mixture consists of $\text{Ce}(\text{OH})_4$ and $\text{Cd}(\text{OH})_2$ crystals coated by a layer of AR14, so that, after calcining the precursor, Cd^{2+} is uniformly distributed in the final product, and the carbon layer is wrapped on its surface. The performance of the photocatalyst was evaluated by the degradation of AR14. The results showed that the photocatalytic efficiency of $\text{Cd-CeO}_2/\text{C}$ was greatly improved due to the formation of a large number of carbon bonds and oxygen vacancies.

2. Experimental

2.1. Chemicals and synthesis

Cerium nitrate hexahydrate ($\text{Ce}(\text{NO}_3)_3 \cdot 6\text{H}_2\text{O}$), potassium iodide

(KI), terephthalic acid (PTA), absolute ethanol ($\text{C}_2\text{H}_6\text{O}$) were purchased from Shanghai Guoyao Reagent Co., Ltd.. Cadmium nitrate tetrahydrate ($\text{Cd}(\text{NO}_3)_2 \cdot 4\text{H}_2\text{O}$) was purchased from Shanghai Jinshanting New Chemical Reagent Factory. Acid Red 14 (AR14, analytical grade) was purchased from Nanjing Chemical Reagent Co., Ltd. 28% ammonia solution ($\text{NH}_3 \cdot \text{H}_2\text{O}$) was purchased from Zhejiang Hannuo Chemical Technology Co., Ltd. P-benzoquinone (BQ, analytical grade) was purchased from Shanghai Puzhen Biotechnology Co., Ltd. All the chemicals were used without further purification.

The synthesis of Cd doped CeO_2 can be described as follows. 1 g of a mixture of $\text{Ce}(\text{NO}_3)_3 \cdot 6\text{H}_2\text{O}$ and a small amount of $\text{Cd}(\text{NO}_3)_2 \cdot 4\text{H}_2\text{O}$ (0.1%, 0.5% and 1%, respectively) was dissolved in 50 mL of deionized water. After stirring for 30 min to dissolve the salts, the pH of the solution was adjusted to 9 by adding $\text{NH}_3 \cdot \text{H}_2\text{O}$, and then the solution was kept under stirring for 1 h and aged for 3 h. The precipitate ($\text{Cd-Ce}(\text{OH})_4$) was then recovered by filtration, washed three times with water and ethanol, and dried at 60°C for 2 h. Finally, the precursor was calcined in N_2 at 600°C for 2 h to synthesize the resulted composite, which was labeled, depending on the Cd content, as 0.1% Cd-CeO_2 , 0.5% Cd-CeO_2 , 1% Cd-CeO_2 , respectively.

The preparation process of 0.5% Cd-CeO_2 -0.01C, 0.5% Cd-CeO_2 -0.02C, 0.5% Cd-CeO_2 -0.03C followed the same route, except that 1 g of $\text{Ce}(\text{NO}_3)_3 \cdot 6\text{H}_2\text{O}$ and 0.5% $\text{Cd}(\text{NO}_3)_2 \cdot 4\text{H}_2\text{O}$ are dissolved in AR14 solutions at different concentrations (0.01, 0.02 and 0.03 mM).

2.2. Characterization

The X-ray diffraction pattern (XRD) was acquired on a Philips PW3040/60 powder diffractometer using $\text{Cu K}\alpha$ ($\lambda = 0.15406$ nm) radiation at 40 kV and 40 mA, over a 2θ interval ranging from 20° to 80° . The elements distribution of the samples was obtained on Hitachi S-4800 scanning electron microscope under the following test conditions: 10 mA current, 5 kV acceleration voltage, and 8 mm workbench height. The Fourier transform infrared spectroscopy (FT-IR) spectra were recorded by a Nicolet Nexus 670 spectrometer with a resolution of 4 cm^{-1} using the KBr pellet method. The solid-state UV-vis DRS was measured by Cary 5000, under a 200–800 nm measurement range. The photoluminescence spectra (PL) were obtained on a Hitachi F-7000 fluorescence spectrophotometer equipped with a commercial 980 nm NIR laser. The electrochemical tests were carried out with a CH Instruments CHI660D electrochemical station in a standard three electrode configuration. X-ray photoelectron spectroscopy (XPS) data was obtained on a Perkin Elmer PHI-5000C ESCA instrument with a sample surface carbon C 1 s (284.8 eV) as internal standard, Al K (E = 1486.5 eV) as excitation source, and 2×10^{-9} mbar as base pressure. The measurements of N_2 adsorption-desorption were performed on a Micromeritics ASAP 2020 apparatus at -196°C , and the specific surface areas of the investigated samples were calculated using the multiple-point Brunauer-Emmett-Teller (BET) method.

2.3. Photocatalysis experiment

The photocatalytic activity of various samples was evaluated by the degradation of AR14. Accordingly, 0.02 g of catalyst was evenly dispersed in 20 mL of 0.15 mM AR14 aqueous solution. The suspensions were first placed in the dark and kept in agitation in a magnetic stirring for 30 min to reach the adsorption-desorption equilibrium. Then a 300 W mercury lamp ($\lambda = 380 \sim 800$ nm) was used as visible light source to irradiate the suspension for 2 h. Every 30 min, 3 mL solution was taken out and centrifuged to remove the photocatalyst. The residual AR14 levels in the filtrates were then analyzed by recording the variations of the absorbance at 516 nm with a UV-vis spectrophotometer (Evolution 500 LC). The degradation rate of AR14(η) was calculated according to Equation (1).

$$\eta = (C_0 - C)/C_0 \quad (1)$$

where C_0 and C are the concentration of AR14 solution before and after photocatalysis, respectively. The concentration of AR14 before and after photocatalysis has been obtained according to the Lambert-Beer law: $A = \epsilon bc$ (ϵ : absorption coefficient, b : width of cuvette, C : concentration of AR14).

3. Results and discussion

3.1. Structural and morphological characterization

Fig. 1 shows the XRD patterns of CeO_2 , $\text{CeO}_2\text{-}0.02\text{C}$, $0.5\%\text{Cd-CeO}_2$ and $0.5\%\text{Cd-CeO}_2\text{-}0.02\text{C}$. According to Fig. 1, the diffraction peaks of all samples correspond to the pattern of CeO_2 with cubic fluorite structure (JCPDS no. 43-1002). No carbon peak is found in the XRD of $\text{CeO}_2\text{-}0.02\text{C}$, which may be caused by the amorphous structure of carbon. The XRD pattern of Cd-doped samples did not show any significant difference, indicating that Cd^{2+} effectively enters CeO_2 lattice and partially replaces Ce^{4+} cations (Gnanam and Rajendran, 2018, Phatthanit et al., 2021). In addition, it can be seen from Fig. 1 that the XRD peak intensity of the samples decreased, and the peak position of (111) crystal plane shifted slightly to a higher angle after doping with Cd^{2+} . This indicates that when Cd^{2+} (0.074 nm) replaces Ce^{4+} (0.092 nm) (Yao et al., 2015, Zhu et al., 2017), the crystal face is depressed and the interplanar spacing becomes smaller, which is consistent with Bragg's law ($2d\sin\theta = n\lambda$), so the diffraction peak shifts to a high diffraction angle (Qi et al., 2019).

The FT-IR spectra of CeO_2 and doped CeO_2 samples, acquired to determine the surface functional groups of the different catalysts, are shown in Fig. 2. It can be seen from Fig. 2 that all samples have evident bands near 500, 1105, 1395, 1640, 3430 cm^{-1} , of which the bands near 500 cm^{-1} are caused by the vibration of Ce-O, Cd-O and Ce-O-Ce, while the characteristic absorption band at 1105 cm^{-1} can be attributed to the vibration of non-bridging Ce-O and Cd-O (Syed et al., 2021). The bands at 3430 and 1640 cm^{-1} are related to the O-H vibration in surface adsorbed water (Gnanam and Rajendran, 2018, Murugadoss et al., 2019). The weak band at 1395 cm^{-1} may be caused by the absorption of CO_2 from the atmosphere (Syed et al., 2021, Wang et al., 2017).

Field emission scanning electron microscopy (SEM) of $0.5\%\text{Cd-CeO}_2\text{-}0.02\text{C}$ is illustrated in Fig. S2, from which it can be seen that the synthesized product exhibits irregular blocky morphology. Other samples have similar morphology to that of $0.5\%\text{Cd-CeO}_2\text{-}0.02\text{C}$ (not shown).

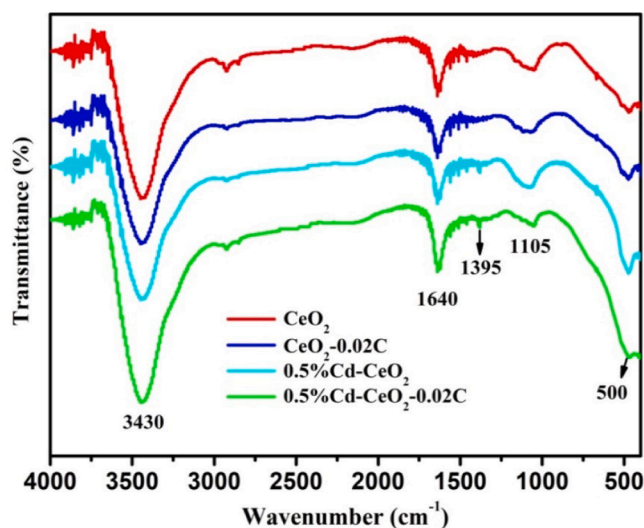


Fig. 2. FT-IR spectra of different catalysts.

Element distribution and EDS spectra of $0.5\%\text{Cd-CeO}_2\text{-}0.02\text{C}$ are shown in Fig. 3. According to Fig. 3 (a)-(d), it can be found that $0.5\%\text{Cd-CeO}_2\text{-}0.02\text{C}$ does contain C, O, Ce, Cd, and that all the elements are evenly distributed in the catalyst. It can be seen from Fig. 3 (e) that the mass ratio and atomic percentage of Cd in the sample are close to the theoretical value of 0.86% and 0.51%, respectively. The mass ratio and atomic percentage of C are 0.88% and 4.84%, respectively, which proved that the adsorbed dye was indeed converted into carbon after calcination. The distribution of elements in other carbon containing samples are similar to that of $0.5\%\text{Cd-CeO}_2\text{-}0.02\text{C}$ (not shown).

The Cd 3d XPS spectra of samples $0.5\%\text{Cd-CeO}_2\text{-}0.01\text{C}$, $0.5\%\text{Cd-CeO}_2\text{-}0.02\text{C}$, $0.5\%\text{Cd-CeO}_2\text{-}0.03\text{C}$ and $0.5\%\text{Cd-CeO}_2$ are shown in Fig. 4. According to Fig. 4, all samples have obvious peaks near 404 and 411 eV, corresponding to the spin of Cd $3d_{5/2}$ and $3d_{3/2}$, respectively (Shanmugam et al., 2019), which proves that Cd^{2+} successfully entered the CeO_2 framework, in agreement with the findings obtained from Fig. 3 (d).

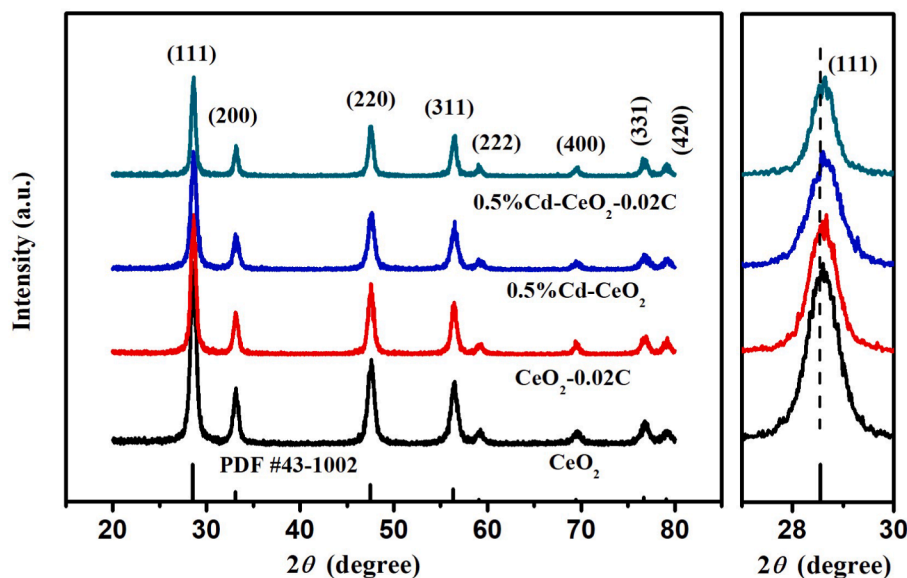


Fig. 1. XRD patterns of CeO_2 , $\text{CeO}_2\text{-}0.02\text{C}$, $0.5\%\text{Cd-CeO}_2$, and $0.5\%\text{Cd-CeO}_2\text{-}0.02\text{C}$.

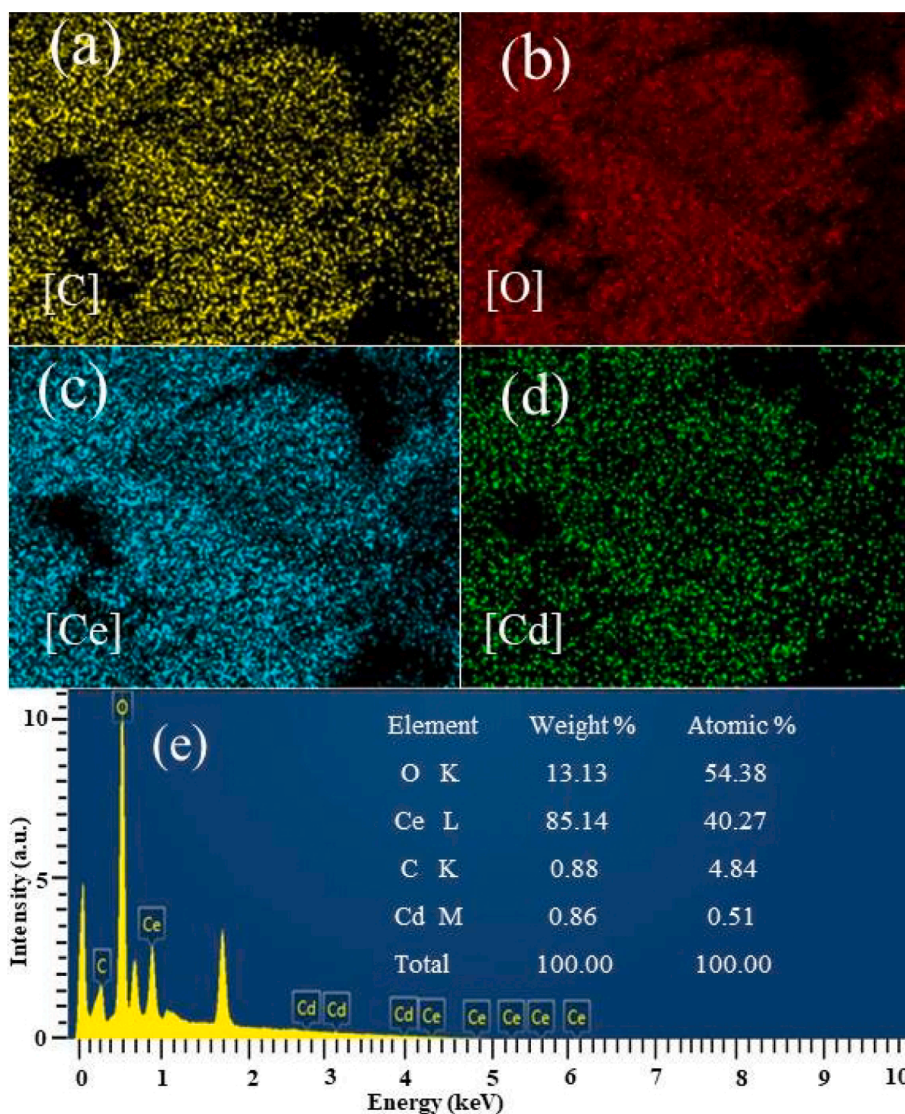


Fig. 3. Element distribution and EDS spectra in 0.5%Cd-CeO₂-0.02C.

3.2. Photocatalytic degradation tests

The results of AR14 photocatalytic degradation tests are shown in Fig. 5. The curves clearly show that the presence of a small amount of Cd is favorable to improve the photocatalytic efficiency of CeO₂. The possible reason is that oxygen vacancies are formed on the surface of the sample after Cd²⁺ replaces Ce³⁺ or Ce⁴⁺ in CeO₂ lattice (see O 2p XPS diagram for details). These oxygen vacancies can easily entrap the photogenerated electrons, reducing the recombination rate of photogenerated electron-hole pairs. As a result, the doped Cd catalysts showed a better catalytic efficiency than that of pure CeO₂. The improvement in the photocatalytic efficiency reaches a maximum for a 0.5% Cd loading, while the 1% Cd sample shows a worse performance. PL tests were carried out to further investigate this effect. The results, shown in Fig. 5 (b), indicate a trend in the PL intensity of the catalysts consistent with that of the photocatalytic degradation tests (Fig. 5 (a)), which proves that Cd doping can indeed inhibit the recombination of photogenerated electrons and holes. As a matter of fact, the intensity of the peak at 435 nm in the PL spectrum (caused by the recombination of conduction band electrons and holes (Choudhary et al., 2020)) is reduced after Cd-doping. The peak intensity of 0.5%Cd-CeO₂ is the lowest, indicating that with 0.5% Cd-doping the best separation efficiency of photogenerated electrons and holes, and then the highest photocatalytic

activity, is obtained. In addition, it can be seen from Fig. 7 that doping of Cd promotes the absorption of light, increasing the yield of photogenerated electrons and thus the photocatalytic efficiency.

After finding the optimal amount of Cd, to evaluate the influence of C content on the photocatalytic efficiency, different catalysts have been synthesized introducing different amounts of AR14 into 0.5%Cd-CeO₂: 0.5%Cd-CeO₂-0.01C, 0.5%Cd-CeO₂-0.02C, 0.5%Cd-CeO₂-0.03C. The photocatalytic activities of the obtained catalysts are shown in Fig. 6 (a) and the results demonstrate that the introduction of C has a great impact on the catalyst activity. Also in this case the amount of C has an optimal value: according to Fig. 6 (b), 0.5%Cd-CeO₂-0.02C promoted an effective degradation of AR14 because the characteristic peaks of this dye (benzene ring vibration peak at 1504 and 1604 cm⁻¹, sulfonic acid group (-SO₃H) vibration peak at 1198 and 1277 cm⁻¹) (Hao et al., 2016) are not found on the recovered catalyst, that shows the same infrared spectrum of the fresh one. From the results of specific surface area (S_{BET}), it can be found that introducing of C is helpful for the improvement of S_{BET} because S_{BET} of 0.5%Cd-CeO₂, 0.5%Cd-CeO₂-0.01C, 0.5%Cd-CeO₂-0.02C, 0.5%Cd-CeO₂-0.03C are 8.6, 46.5, 53.1, 43.6 m²/g, respectively. Generally, the higher S_{BET}, the greater the adsorption capacity. Therefore, introducing of C is benefit to improve the photocatalytic efficiency of the resulted samples.

It is obvious from Fig. S3 (a) that pH value has a great effect on the

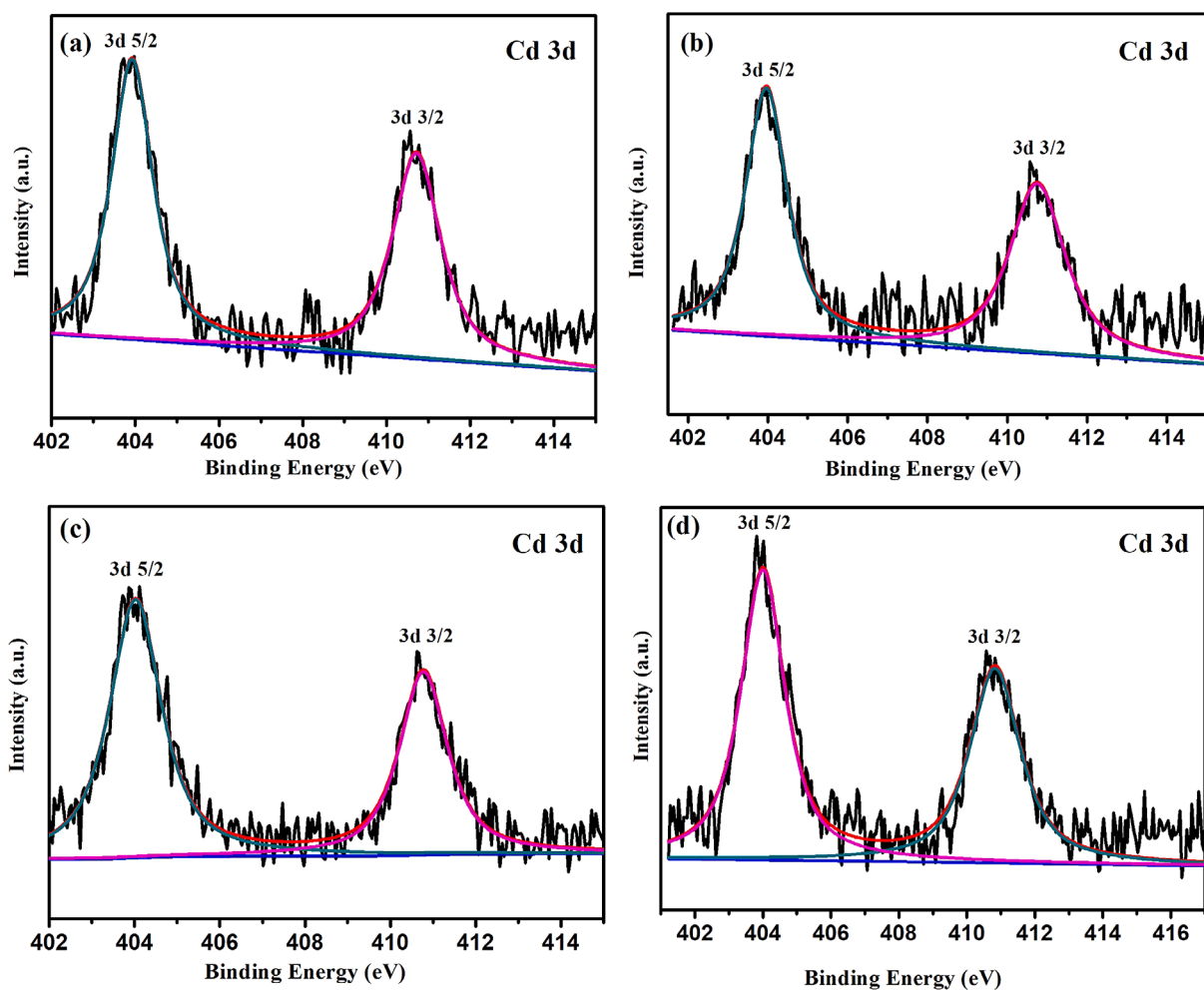


Fig. 4. Cd 3d deconvolution XPS spectra of (a) 0.5%Cd-CeO₂-0.01C, (b) 0.5%Cd-CeO₂-0.02C, (c) 0.5%Cd-CeO₂-0.03C, (d) 0.5%Cd-CeO₂.

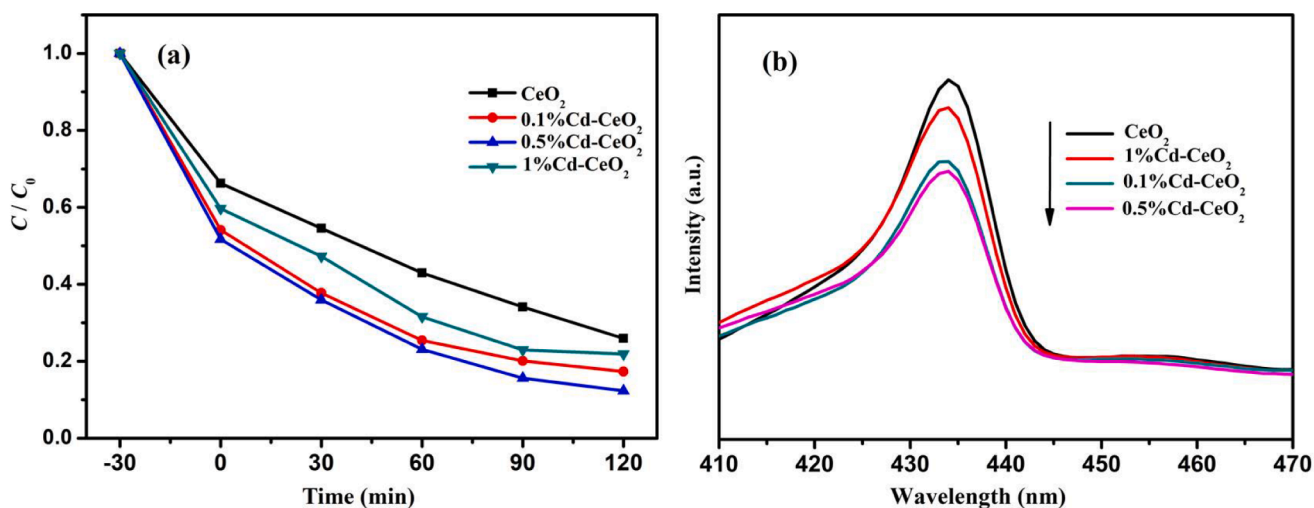


Fig. 5. Photocatalytic degradation efficiency of AR14 (a) and photoluminescence spectra (b) of CeO₂, 0.1%Cd-CeO₂, 0.5%Cd-CeO₂ and 1%Cd-CeO₂.

photocatalytic efficiency of AR14 over 0.5%Cd-CeO₂-0.02C and that the photocatalytic efficiency decrease gradually with increase of pH value. The reason may be that acidic media is conducive to the protonation of hydroxyl groups on the surface of 0.5%Cd-CeO₂-0.02C, which is helpful for improving the adsorption of AR14 due to the formation of electrostatic interactions between the sulfonic acid group in AR14 and the

protonated hydroxyl groups on the surface of photocatalyst. It can be seen from Fig. S3 (b) that the photocatalytic efficiency decrease gradually with increase of AR14 dosage.

The reuse performance of 0.5%Cd-CeO₂-0.02C is shown in Fig. S4 (a). It can be seen from Fig. S4 (a) that the photocatalytic efficiency of AR14 for 0.5%Cd-CeO₂-0.02C remains basically unchanged after 5 times

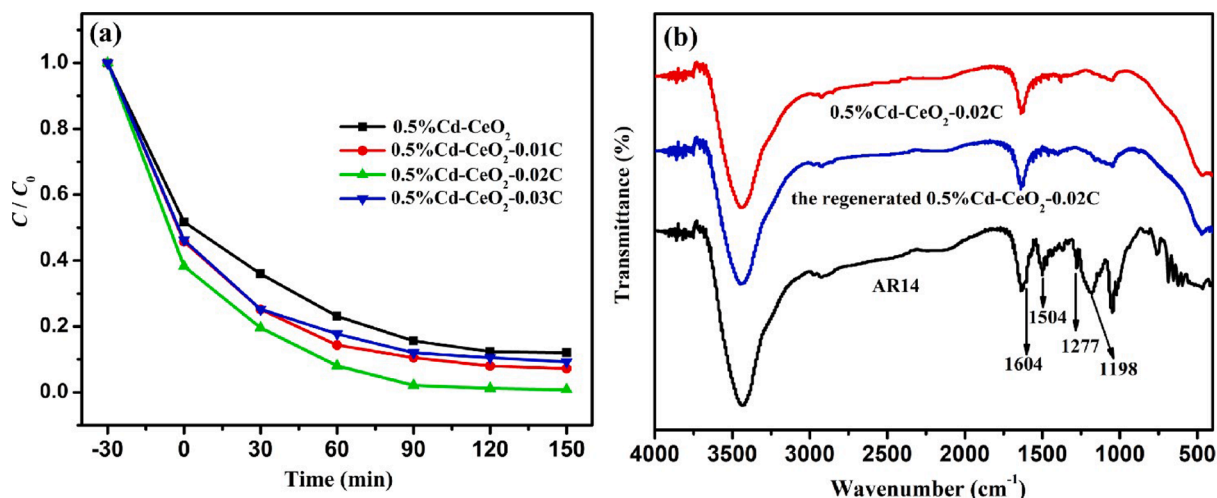


Fig. 6. Photocatalytic degradation efficiency of AR14 by 0.5%Cd-CeO₂, 0.5%Cd-CeO₂-0.01C, 0.5%Cd-CeO₂-0.02C, 0.5%Cd-CeO₂-0.03C (a) and FT-IR spectra of AR14 and 0.5%Cd-CeO₂-0.02C (before and after photodegradation) (b).

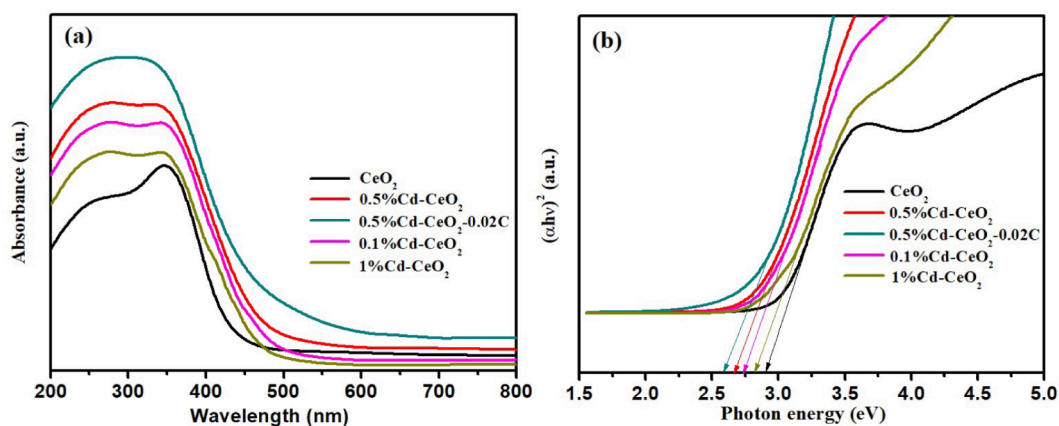


Fig. 7. Diffuse reflectance UV-vis spectra (a), optical absorption edges (b) of different catalysts.

of repeated use, implying that the photocatalyst has a good reusability. It can be concluded from Fig. S4 (b) that 0.5%Cd-CeO₂-0.02C has a high stability because the structure of the fresh photocatalyst is similar to that of after 5 photocatalytic cycles.

3.3. Study of the photocatalytic mechanism

The UV-vis diffuse reflectance spectra of CeO₂, 0.1%Cd-CeO₂, 0.5% Cd-CeO₂, 1%Cd-CeO₂ and 0.5%Cd-CeO₂-0.02C is shown in Fig. 7 (a). According to Fig. 7 (a), it can be found that, after Cd-doping, the sample not only increases the absorption of UV radiation, but also extends the

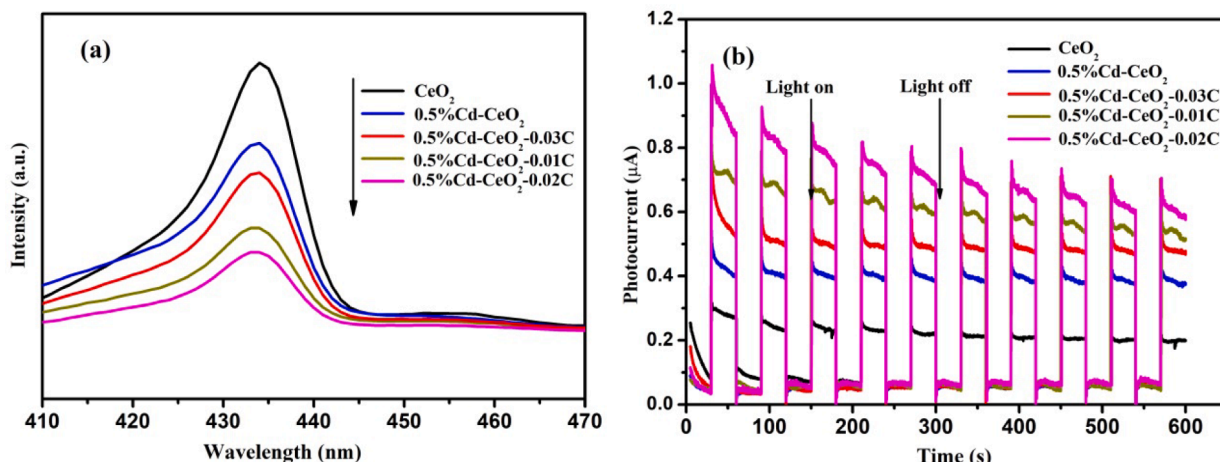


Fig. 8. Photoluminescence spectra (a) and photocurrent spectra (b) of different catalysts.

absorption band to a higher wavelength limit, making the Cd-doped samples sensitive to visible light, and thus resulting in the improvement of light absorption efficiency. The band gap of each sample can be estimated by extrapolating the linear region of the plot of $(\alpha h\nu)^2$ versus $h\nu$ (Murugadoss et al., 2019). According to the results, shown in Fig. 7 (b), the optical band gap energies of the doped samples are lower than that of CeO_2 , which leads to the improvement of their photocatalytic efficiency.

Photoluminescence and photocurrent techniques are usually used to investigate the separation of photogenerated electrons and holes. Fig. 8 (a) shows the photoluminescence spectra of CeO_2 , 0.5% Cd-CeO_2 , 0.5% $\text{Cd-CeO}_2\text{-0.01C}$, 0.5% $\text{Cd-CeO}_2\text{-0.02C}$, 0.5% $\text{Cd-CeO}_2\text{-0.03C}$. According to Fig. 8 (a), the photoluminescence intensity of 0.5% Cd-CeO_2 decreases after introduction of C, indicating that the recombination rate of photogenerated electrons and holes is reduced, which improves the lifetime of photogenerated carriers (Wang et al., 2020). Fig. 8 (a) suggests that the separation efficiency of photogenerated electrons and holes increases along the following sequence: 0.5% $\text{Cd-CeO}_2\text{-0.02C}$, 0.5% $\text{Cd-CeO}_2\text{-0.01C}$, 0.5% $\text{Cd-CeO}_2\text{-0.03C}$, 0.5% Cd-CeO_2 , CeO_2 . To prove this evidence, photocurrent experiments were carried out and the results are shown in Fig. 8 (b). Generally, the higher the photocurrent intensity, the higher the separation efficiency of photogenerated electrons and holes (Xu et al., 2020). According to Fig. 8 (b), the behavior of all samples is also consistent with the photoluminescence results. Moreover, being the highest photocurrent intensity for 0.5% $\text{Cd-CeO}_2\text{-0.02C}$, it can be found that the photocatalytic efficiency of 0.5% Cd-CeO_2 is further improved after introduction of C.

Several important information, such as elemental composition and chemical state of the sample surface, can be investigated by X-ray photoelectron spectroscopy (XPS). Therefore, XPS tests were carried out

for 0.5% $\text{Cd-CeO}_2\text{-0.01C}$, 0.5% $\text{Cd-CeO}_2\text{-0.02C}$, 0.5% $\text{Cd-CeO}_2\text{-0.03C}$ and 0.5% Cd-CeO_2 , respectively. Fig. 9 shows the C 1s XPS spectra of different samples. All samples have evident peaks at 284.0, 284.4, 284.9, 286.2 and 288.3 eV, which can be attributed to C = C, C-C, C-OH, C = O and O = C-O bonds (Pérez-González and Tomás, 2021), indicating that the carbon deriving from the dye pyrolysis is successfully combined with the matrix. The formation of carbon bond is beneficial to the transmission of photogenerated electrons, thus improving the separation efficiency of photogenerated electrons and holes and enhancing the photocatalytic efficiency (Ye et al., 2019). Because the formation of a large number of carbon bonds can promote the separation of photogenerated electrons and holes, the PL intensity of the corresponding synthetic products decreases and the photogenerated current intensity increases. The carbon bond peak areas of 0.5% $\text{Cd-CeO}_2\text{-0.01C}$, 0.5% Cd-

Table 1
Peak areas of carbon bonds in different photocatalysts.

Peak Type	C-C	C = C	C-OH	C = O	O-C=O	Total area
Sample						
0.5% $\text{Cd-CeO}_2\text{-0.01C}$	3677.49	3933.81	4506.54	1412.46	7504.21	21034.51
0.5% $\text{Cd-CeO}_2\text{-0.02C}$	2585.99	4093.24	4257.85	5170.67	9356.37	25464.12
0.5% $\text{Cd-CeO}_2\text{-0.03C}$	1492.26	4247.15	3194.82	1941.13	5709.20	16584.56

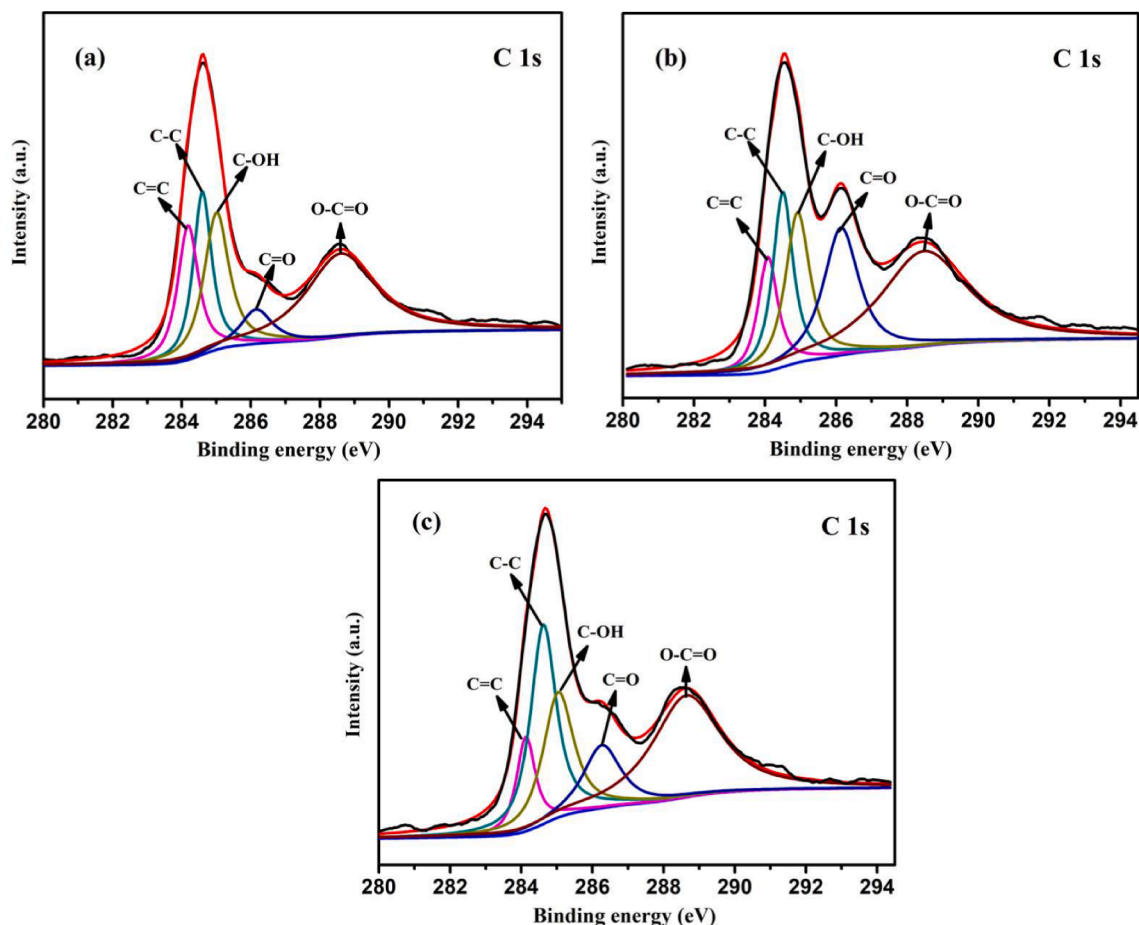


Fig. 9. C 1s XPS spectra of (a) 0.5% $\text{Cd-CeO}_2\text{-0.01C}$, (b) 0.5% $\text{Cd-CeO}_2\text{-0.02C}$, (c) 0.5% $\text{Cd-CeO}_2\text{-0.03C}$.

CeO₂-0.02C and 0.5%Cd-CeO₂-0.03C are shown in Table 1. The results are, once again, consistent with the photocatalytic data. In fact, the total carbon bond peak area, and so the number of C bonds, of 0.5%Cd-CeO₂-0.02C is the largest, according to the best photocatalytic activity showed by this sample, and the same holds for the other two samples. It can be seen from table 1 that the peak areas of O = C-O and O = C in 0.5%Cd-CeO₂-0.02C are higher than those in 0.5%Cd-CeO₂-0.01C and 0.5%Cd-CeO₂-0.03C, which may be explain the fact that introducing moderate AR14 in the precursor can increase the number of carbon bonds and thus improve the photocatalytic efficiency of the resulted sample.

Fig. 10 shows the Ce 3d XPS spectra of different samples. The spectra have been deconvoluted into a total of 10 peaks. In order to determine the specific valence of Ce (Ce³⁺ and Ce⁴⁺), the multiple state splitting of the spin orbitals of Ce 3d_{3/2} and Ce 3d_{5/2} were labeled as U and V. It is reported that the peaks marked V₀, V', U₀, U' belong to Ce³⁺, and the peaks marked U, V, U'', V'', U''', V''' belong to Ce⁴⁺ (Zarkov et al., 2017). According to the fitting results, such peaks appear in the Ce 3d XPS spectra of all samples, revealing that Ce³⁺ and Ce⁴⁺ are always present. It is reported that the presence of Ce³⁺ can produce charge imbalance, vacancy and unsaturated chemical bands on the catalyst surface, resulting in the change of O (1 s) chemical state and the increase of oxygen chemisorption, that leads to the formation of active species to degrade organic pollutants (Gao et al., 2010, Yang et al., 2006). Therefore, the higher the proportion of Ce³⁺ in the sample, the better the photocatalytic activity. The peak area and content of Ce³⁺ in different photocatalysts are presented in Table 2. It can be seen from Table 2 that the Ce³⁺ content of 0.5%Cd-CeO₂-0.02C is the highest, leading to the

highest oxygen vacancy concentration and thus the highest photocatalytic efficiency. According to the data in Table 2, the order of Ce³⁺ content in each catalyst is consistent with its photocatalytic efficiency, which further proves the important role of Ce³⁺ in photocatalytic efficiency. Ce³⁺ content is calculated by the following formula (where Uⁱ and Vⁱ represent the relevant peak area):

$$C_{Ce^{(III)}} = \frac{v' + u' + v_0 + u_0}{\sum_i (v^i + u^i)} \times 100\%$$

Fig. 11 shows the O1s XPS spectra of different photocatalysts. All samples have peaks at binding energies of about 529, 531 and 533 eV, which can be attributed to lattice oxygen (OI), surface hydroxyl oxygen (OII) and bridging oxygen (OIII) in metal oxides (Qian et al., 2017, Jilani et al., 2021). According to the peak area ratio of the three oxygen species, the relative percentages of the three oxygen species can be quantified, which is shown in Table 3. From the data in Table 3, it can be found that the proportion of lattice oxygen decreases, while the proportion of hydroxyl oxygen and bridging oxygen increases after introduction of carbon. The increase of hydroxyl oxygen content leads to the improvement of the adsorption efficiency of photocatalyst for organic pollutants, resulting in the improvement of photocatalysis efficiency. It can be concluded from the values in Table 3 that the hydroxyl oxygen content of each sample is related to its photocatalytic efficiency. The hydroxyl oxygen content of sample 0.5%Cd-CeO₂-0.02C is the highest, confirming once again its role in the photocatalysis process.

From the results of Fig. S5 and S6, it can be concluded that hydroxyl radical is mainly responsible for the degradation of AR14. Based on the

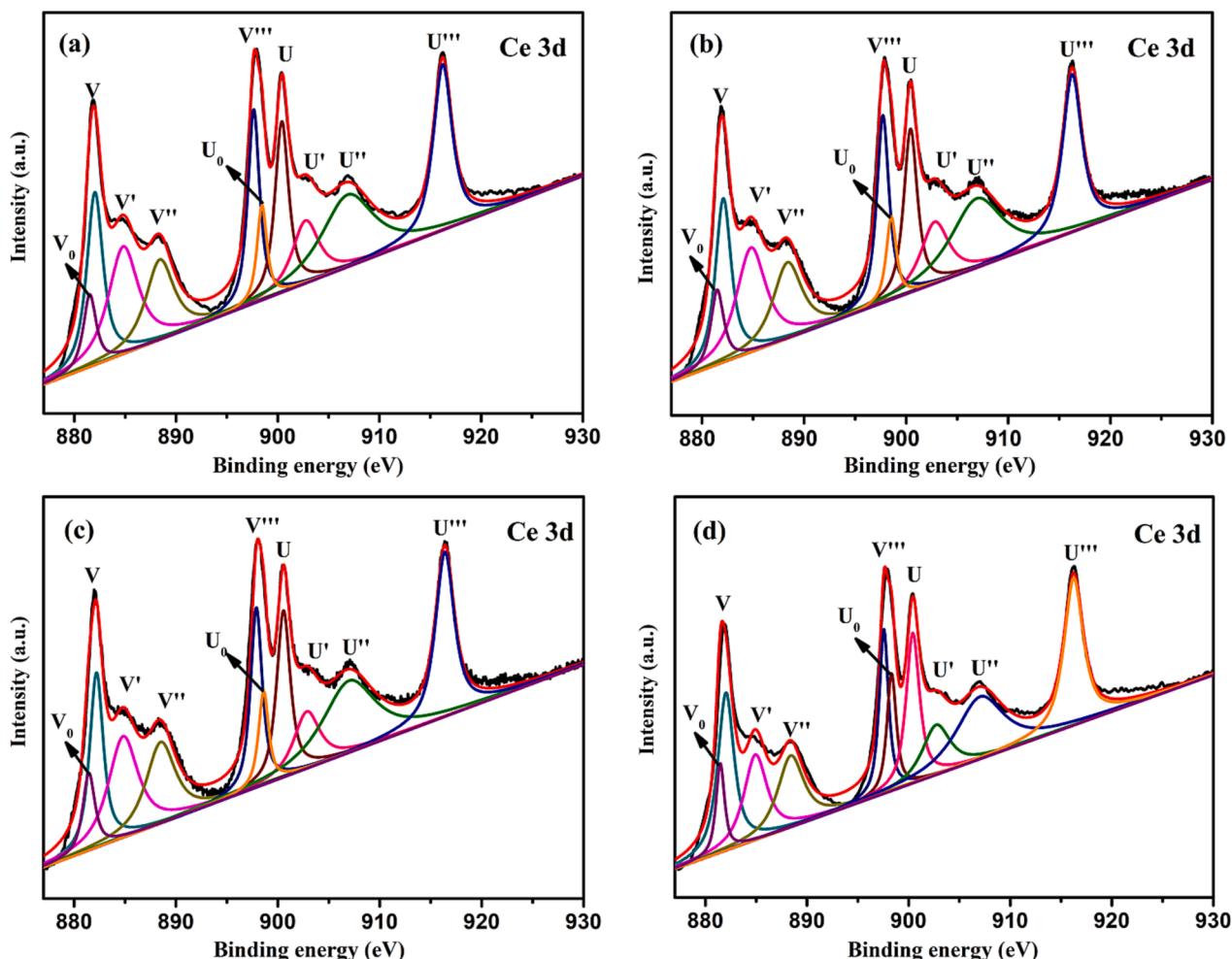
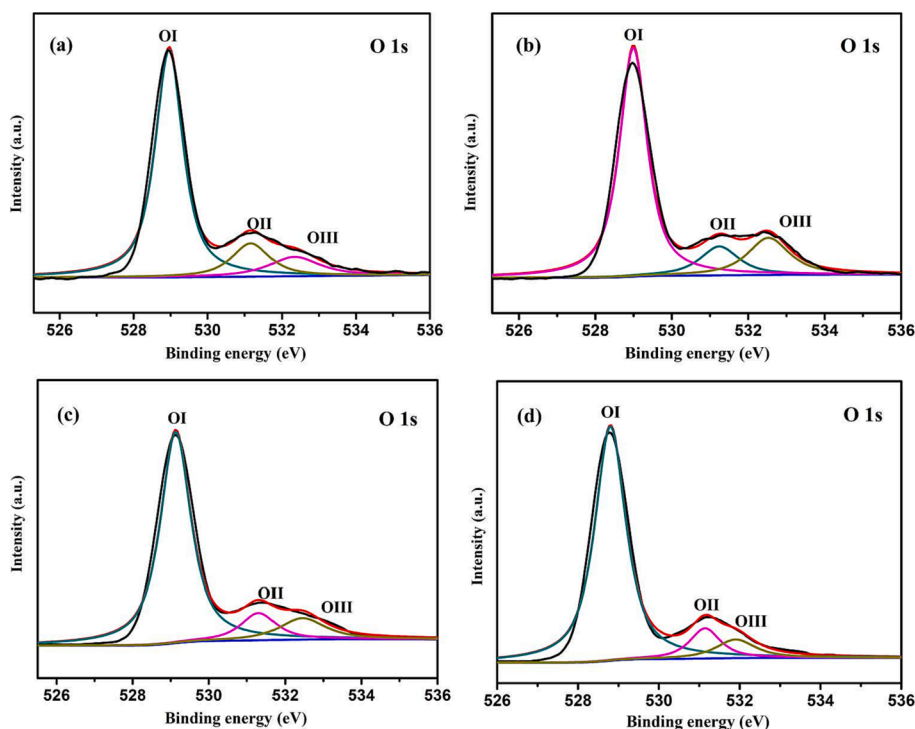


Fig. 10. Ce 3d XPS spectra of (a) 0.5%Cd-CeO₂-0.01C, (b) 0.5%Cd-CeO₂-0.02C, (c) 0.5%Cd-CeO₂-0.03C and (d) 0.5%Cd-CeO₂.

Table 2Peak areas and content of Ce^{3+} of different photocatalysts.

Peak Type	V_0	V'	U_0H	U'	Total area	Content of Ce^{3+}
Sample						
0.5%Cd-CeO ₂ -0.01C	33858.1	117362.1	34279.8	60815.0	851060.9	28.9%
0.5%Cd-CeO ₂ -0.02C	37087.1	118703.6	31799.2	65960.0	861913.7	29.4%
0.5%Cd-CeO ₂ -0.03C	30137.1	96580.0	30412.4	47264.7	716229.5	28.5%
0.5%Cd-CeO ₂	20222.1	52259.6	29335.9	36983.7	504964.7	27.5%

**Fig. 11.** O 1s XPS spectra of (a) 0.5%Cd-CeO₂-0.01C, (b) 0.5%Cd-CeO₂-0.02C, (c) 0.5%Cd-CeO₂-0.03C and (d) 0.5%Cd-CeO₂.**Table 3**

Oxygen species content of different photocatalysts.

Peak Type	OI	OII	OIII
Sample			
0.5%Cd-CeO ₂ -0.01C	74.71%	12.66%	12.63%
0.5%Cd-CeO ₂ -0.02C	69.40%	14.86%	15.74%
0.5%Cd-CeO ₂ -0.03C	76.91%	11.41%	11.68%
0.5%Cd-CeO ₂	81.46%	10.35%	8.20%

above experimental results and analysis, the photocatalytic degradation mechanism of AR14 over Cd-CeO₂@C is illustrated and presented in Fig. S7.

4. Conclusion

In this study, Cd²⁺, Ce³⁺ and AR14 were used as raw materials to synthesize Cd-Ce(OH)₄@AR14 precursor by a coprecipitation method, and Cd-CeO₂@C was obtained via the calcination of the precursor in inert atmosphere. The results of photocatalysis tests showed that Cd-CeO₂@C with a proper amount of Cd and C has a high photocatalytic efficiency, and the main reasons are presented as follows. First, doping with Cd²⁺ can effectively reduce the band gap of CeO₂ and improve the utilization efficiency of light radiation. Second, the formation of carbon bonds can promote the separation of photogenerated electron-hole pairs. Third, the introduction of carbon and Cd²⁺ is helpful for the

reduction of Ce⁴⁺ to Ce³⁺ and thus the formation of oxygen vacancies.

Declaration of Competing Interest

The authors declare that they have no known competing financial interests or personal relationships that could have appeared to influence the work reported in this paper.

Acknowledgements

The financial support by the National Natural Science Foundation of China (21876158) is gratefully acknowledged.

Appendix A. Supplementary data

Supplementary data to this article can be found online at <https://doi.org/10.1016/j.arabjc.2023.105496>.

References

- Azghandi, M.H.A., Vasheghani, F.B., Rajabi, F.H., Keramati, M., 2017. Synthesis of Cd doped ZnO/CNT nanocomposite by using microwave method: Photocatalytic behavior, adsorption and kinetic study. *Results. Phys.* 7, 1106–1114.
- Bello, O.S., Adegoke, K.A., Olaniyan, A.A., Abdulazeez, H., 2015. Dye adsorption using biomass wastes and natural adsorbents: overview and future prospects. *Desalin. Water. Treat.* 53, 1292–1315.

- Bilińska, L., Gmurek, M., Ledakowicz, S., 2016. Comparison between industrial and simulated textile wastewater treatment by AOPs-Biodegradability, toxicity and cost assessment. *Chem. Eng. J.* 306, 550–559.
- Bueno-Alejo, C.J., Grausa, J., Arenal, R., Lafuente, M., Bottega-Pergher, B., Hueso, J.L., 2021. Anisotropic Au-ZnO photocatalyst for the visible-light expanded oxidation of n-hexane. *Catal. Today.* 362, 97–103.
- Choudhary, S., Sahu, K., Bisht, A., Singhal, R., Mohapatra, S., 2020. Template-free and surfactant-free synthesis of CeO₂ nanodiscs with enhanced photocatalytic activity. *Appl. Surf. Sci.* 503, 144102.
- Elumalai, P., Parthipan, P., Huang, M.Z., Muthukumar, B., Cheng, L., Govarthanam, M., 2021. A Rajasekar, Enhanced biodegradation of hydrophobic organic pollutants by the bacterial consortium: Impact of enzymes and biosurfactants. *Environ. Pollut.* 289, 117956.
- Fang, S.M., Xin, Y.J., Ge, L., Han, C.C., Qiu, P., Wu, L.E., 2015. Facile synthesis of CeO₂ hollow structures with controllable morphology by template-engaged etching of Cu₂O and their visible light photocatalytic performance. *Appl. Catal. B-Environ.* 179, 458–467.
- Gao, X., Jiang, Y., Zhong, Y., Luo, Z.Y., Cen, K.F., 2010. The activity and characterization of CeO₂-TiO₂ catalysts prepared by the sol-gel method for selective catalytic reduction of NO with NH₃. *J. Hazard. Mater.* 174, 734–739.
- Gnanam, S., Rajendran, V., 2018. Facile sol-gel preparation of Cd-doped cerium oxide (CeO₂) nanoparticles and their photocatalytic activities. *J. Alloy. Compd.* 735, 1854–1862.
- Hao, S.Y., Hou, J., Aprea, P., Deng, H.X., 2016. Amino-functionalized ceria with enhanced daylight photocatalytic efficiency. *Ceram. Int.* 42, 7440–7446.
- Jilani, A., Hussain, S.Z., Ansari, M.O., Kuamr, R., Dustgeer, M.R., Othman, M.H.D., Barakat, M.A., Melaibari, A.A., 2021. Facile synthesis of silver decorated reduced graphene oxide@zinc oxide as ternary nanocomposite: an efficient photocatalyst for the enhanced degradation of organic dye under UV-visible light. *J. Mater. Sci.* 56, 7434–7450.
- Karimi, M.A., Atashkadi, M., Ranjbar, M., Habibi-Yangjeh, A., 2020. Novel visible-light-driven photocatalyst of NiO/Cd/g-C₃N₄ for enhanced degradation of methylene blue. *Arab. J. Chem.* 13, 5810–5820.
- Kumar, R., Umar, A., Kumar, R., Dana, D., Chauhan, M.S., 2021. Low-temperature synthesis of cadmium-doped zinc oxide nanosheets for enhanced sensing and environmental remediation applications. *J. Alloy. Compd.* 863, 158649.
- Ma R., Zhang S., Wen T., Gu P.C., Li L., Zhao G.X., Niu F.L., Huang Q.F., Tang Z.W., Wang X.K. 2019. A critical review on visible-light-response CeO₂-based photocatalysts with enhanced photooxidation of organic pollutants. *Catal. Today.* 335, 20–30.
- Miao, H., Huang, G.F., Liu, J.H., Zhou, B.X., Pan, A., Huang, W.Q., Huang, G.F., 2016. Origin of enhanced photocatalytic activity of F-doped CeO₂ nanocubes. *Appl. Surf. Sci.* 370, 427–432.
- Murali, A., Lan, Y.P., Sarswat, P.K., Free, M.L., 2019. Synthesis of CeO₂/reduced graphene oxide nanocomposite for electrochemical determination of ascorbic acid and dopamine and for photocatalytic applications. *Mater. Today. Chem.* 12, 222–232.
- Murugadoss, G., Ma, J.L., Ning, X.F., Kumar, M.R., 2019. Selective metal ions doped CeO₂ nanoparticles for excellent photocatalytic activity under sun light and supercapacitor application. *Inorg. Chem. Commun.* 109, 107577.
- Pérez-González, M., Tomás, A.Z., 2021. Surface chemistry of TiO₂-ZnO thin films doped with Ag. Its role on the photocatalytic degradation of methylene blue. *Catal. Today.* 360, 129–137.
- Phatranit, D., Aunkorn, P., Somchai, T., Titipun, T., 2021. Photocatalysis of Cd-doped ZnO synthesized with precipitation method. *Rare Metals.* 40, 537–546.
- Qi, Y., Ye, J.W., Zhang, S.Q., Tian, Q.Z., Xu, N., Tian, P., Ning, G.L., 2019. Controllable synthesis of transition metal ion-doped CeO₂ micro/nanostructures for improving photocatalytic performance. *J. Alloy. Compd.* 782, 780–787.
- Qian, J.C., Cao, Y.Y., Chen, Z.G., Liu, C.B., Lu, X.W., 2017. Biomimetic synthesis of cerium oxide nanosquares on RGO and their enhanced photocatalytic activities. *Dalton T.* 46, 547.
- Qian, J.C., Chen, Z.G., Sun, H., Chen, F., Xu, X., Wu, Z.Y., Li, P., Ge, W.J., 2018. Enhanced photocatalytic H₂ production on three-dimensional porous CeO₂/Carbon nanostructure. *ACS. Sustain. Chem. Eng.* 6, 9691–9698.
- Rashidi, H.R., Sulaiman, N.M.N., Hashim, N.A., Hassan, C.R.C., Ramli, M.R., 2015. Synthetic reactive dye wastewater treatment by using nano-membrane filtration. *Desalin. Water. Treat.* 55, 86–95.
- Shanmugam, V., Sanjeevamuthu, S., Jeyaperumal, K.S., Vairamuthu, R., Pitchai, R.I.D., 2019. Highly efficient visible light photocatalytic and antibacterial performance of PVP capped Cd:Ag: ZnO photocatalyst nanocomposites. *Appl. Surf. Sci.* 479, 914–929.
- Subramanyam, K., Sreelekha, N., Reddy, D.A., Ramanadha, M., Poornaprakash, B., Reddy, K.C., Vijayalakshmi, R.P., 2020. Influence of transition metals co-doping on CeO₂ magnetic and photocatalytic activities. *Ceram. Int.* 46, 5086–5097.
- Syed, A., Elgorban, A.M., Alkheraif, A.A., 2021. High performance nanohybrid CeO₂@2D CdO plates with suppressed charge recombination: Insights of photoluminescence, visible-light photocatalysis, intrinsic mechanism and antibacterial activity. *Opt. Mater.* 121, 111510.
- Tahir, M.B., Sagir, M., Abas, N., 2019. Enhanced photocatalytic performance of CdO-WO₃ composite for hydrogen production. *Int. J. Hydrogen Energ.* 44, 24690–24697.
- Velusamy, S., Roy, A., Sundaram, S., Mallick, T.K., 2021. A review on heavy metal ions and containing dyes removal through graphene oxide-based adsorption strategies for textile wastewater treatment. *Chem. Rec.* 21, 1570–1610.
- Wang, K.Q., Guan, Z.Y., Liang, X.Y., Song, S.Y., Lu, P.Y., Zhao, C.R., Yue, L., Zeng, Z.H., Wu, Y., He, Y.M., 2023. Remarkably enhanced catalytic performance in CoO_x/Bi₄Ti₃O₁₂ heterostructures for methyl orange degradation via piezocatalysis and piezo-photocatalysis. *Ultrason Sonochem.* 100, 106616.
- Wang, H., Shang, J., Xiao, Z.L., Aprea, P., Hao, S.Y., 2020. Novel construction of carbon bonds in CeO₂@C with efficiently photocatalytic activity. *Dyes. Pigments.* 182, 108669.
- Wang, W., Zhu, Q., Dai, Q.G., Wang, X.Y., 2017. Fe doped CeO₂ nanosheets for catalytic oxidation of 1, 2-dichloroethane: Effect of preparation method. *Chem. Eng. J.* 307, 1037–1046.
- Xu, F.H., Lai, C., Zhang, M.M., Li, B.S., Liu, S.Y., Chen, M., Li, L., Xu, Y., Qin, L., Fu, Y.K., Liu, X.G., Yi, H., Yang, X.F., 2021. Facile one-pot synthesis of carbon self-doped graphitic carbon nitride loaded with ultra-low ceric dioxide for high-efficiency environmental photocatalysis: Organic pollutants degradation and hexavalent chromium reduction. *J. Colloid. Interf. Sci.* 601, 196–208.
- Xu, J., Li, M., Qiu, J.H., Zhang, X.F., Feng, Y., Yao, J.F., 2020. Pegylated deep eutectic solvent-assisted synthesis of CdS@CeO₂ composites with enhanced visible light photocatalytic ability. *Chem. Eng. J.* 380, 123135.
- Yang, S.X., Zhu, W.P., Jiang, Z.P., Chen, Z.X., Wang, J.B., 2006. The surface properties and the activities in catalytic wet air oxidation over CeO₂-TiO₂ catalysts. *Appl. Surf. Sci.* 252, 8499–8505.
- Yao, Y.J., Chen, H., Lian, C., Wei, F.Y., Zhang, D.W., Wu, G.D., Chen, B.J., Wang, S.B., 2016. Fe Co, Ni nanocrystals encapsulated in nitrogen-doped carbon nanotubes as Fenton-like catalysts for organic pollutant removal. *J. Hazard. Mater.* 314, 129–139.
- Yao, G., Tang, Y.Q., Fu, Y.J., Jiang, Z.Q., An, X.Y., Chen, Y., Liu, Y.D., 2015. Fabrication of high-quality ZnCdO epilayers and ZnO/ZnCdO heterojunction on sapphire substrates by pulsed laser deposition. *Appl. Surf. Sci.* 326, 271–275.
- Ye, K.H., Yang, H., Li, M.Y., Huang, Y.C., Zhang, S.Q., Ji, H.B., 2019. An ultrathin carbon layer activated CeO₂ heterojunction nanorods for photocatalytic degradation of organic pollutants. *Appl. Catal. B-Environ.* 259, 118085.
- Zarkov, A., Stanulis, A., Mikoliunaite, L., Katelnikovas, A., Jasulaitiene, V., Ramanauskas, R., Tautkus, S., Kareiva, A., 2017. Chemical solution deposition of pure and Gd-doped ceria thin films: Structural, morphological and optical properties. *Ceram. Int.* 43, 4280–4287.
- Zeng, M., Li, Y.Z., Mao, M.Y., Bai, J.L., Ren, L., Zhao, X.J., 2015. Synergetic effect between photocatalysis on TiO₂ and thermocatalysis on CeO₂ for gas-phase oxidation of benzene on TiO₂/CeO₂ nanocomposites. *ACS Catal.* 5, 3278–3286.
- Zhang, J.Y., Zhang, W.Q., Yue, L., Hu, X., Lin, H.J., Zhao, L.H., He, Y.M., 2022. Thiophene insertion and lanthanum molybdate modification of g-C₃N₄ for enhanced visible-light-driven photoactivity in tetracycline degradation. *Appl. Surf. Sci.* 592, 153337.
- Zhu, H.J., Xu, J., Yichuan, Y.G., Wang, Z.P., Gao, Y.B., Liu, W., Yin, H.N., 2017. Catalytic oxidation of soot on mesoporous ceria-based mixed oxides with cetyltrimethyl ammonium bromide (CTAB)-assisted synthesis. *J. Colloid. Interf. Sci.* 508, 1–13.
- Zhuang, J.D., Tian, Q.F., Liu, Q., Liu, P., Cui, X.R., Li, Y.Q., Fan, M.Z., 2017. New insight into binary TiO₂@C nanocomposites: the crucial effect of an interfacial microstructure. *Phys. Chem. Chem. Phys.* 19, 9519.